Near Surface Geophysics, 2009, 629-646

A review of helicopter-borne electromagnetic methods for groundwater exploration

Bernhard Siemon[1*], Anders Vest Christiansen[3] and Esben Auken[2]

[1] *Federal Institute for Geosciences and Natural Resources (BGR), Stilleweg 2, 30655 Hannover, Germany*
[2] *The HydroGeophysics Group, Department of Earth Sciences, University of Aarhus (HGG), Høegh-Guldbergs Gade 2, 8000 Aarhus C, Denmark*
[3] *Geological Survey of Denmark and Greenland (GEUS), Lyseng Allee 1, 8270 Højbjerg, Denmark*

Received October 2008, revision accepted July 2009

ABSTRACT

For about three decades, airborne electromagnetic (AEM) systems have been used for groundwater exploration purposes. Airborne systems are appropriate for large-scale and efficient groundwater surveying. Due to the dependency of the electrical conductivity on both the clay content of the host material and the mineralization of the water, electromagnetic systems are suitable for providing information about the aquifer structures and water quality, respectively.

More helicopter than fixed-wing systems are used in airborne groundwater surveys. Helicopter-borne frequency-domain electromagnetic (HEM) systems use a towed rigid-boom. Helicopter-borne time-domain (HTEM) systems, which use a large transmitter loop and a small receiver within or above the transmitter, are generally designed for mineral exploration purposes but recent developments have made some of these systems usable for groundwater purposes as well.

The quantity measured, the secondary magnetic field, depends on the subsurface conductivity distribution. Due to the skin-effect, the penetration depths of the AEM fields depend on the system characteristics used: high-frequency data/early-time channels describe the shallower parts of the conducting subsurface and the low-frequency data/late-time channels the deeper parts. Typical investigation depths range from some ten metres (conductive grounds) to several hundred metres (resistive grounds), where the HEM systems are appropriate for shallow to medium deep (about 1–100 m) and the HTEM systems for medium deep to deep (about 10–400 m) investigations.

Generally, the secondary field values are inverted into resistivities and depths using homogeneous or layered half-space models. As the footprint of AEM systems is rather small, one-dimensional interpretation of AEM data is sufficient in most cases and single-site inversion procedures are widely used. Laterally constrained inversion of AEM data often improves the stability of the inversion models, particularly for noisy data. Higher dimensional inversion is still not possible for standard-size surveys.

Based on typical field examples the advantages as well as the limitations of AEM surveys compared to long-established ground-based geophysical methods used in groundwater surveys are discussed. In a case history from a German island an airborne frequency-domain system is used to successfully locate freshwater lenses on top of saltwater. An example from Denmark shows how a time-domain system is used to locate large-scale buried structures forming ideal groundwater aquifers.

INTRODUCTION

Large-scale groundwater surveys increasingly apply airborne geophysical methods in order to investigate huge areas in reasonable time and at relatively low costs. From the most common airborne methods currently utilized – magnetics, radiometrics and electromagnetics, which are generally used simultaneously – airborne electromagnetics (AEM) contributes most to groundwater exploration purposes due to the dependency of the electrical conductivity on a) the salinity of the groundwater, i.e., the groundwater quality, and b) the clay content of the subsurface, i.e., the aquifer conditions and protection level (e.g., Kirsch 2006).

The application of geoelectrical and electromagnetic methods on ground (e.g., McNeill 1990; Binley and Kemna 2005; Everett and Meju 2005; Ernstson and Kirsch 2006) has a long tradition in groundwater exploration. AEM, however, was introduced for mineral exploration and – compared to that – airborne groundwater exploration is rather new. Although the first tests on the applicability of airborne systems for hydrogeological investiga-

* bernhard.siemon@bgr.de

tions date back to 1965 (Baudouin *et al.* 1967; Collett 1967), airborne geophysics was not a sufficient tool for groundwater exploration at that time. One of the first successful groundwater investigation surveys was conducted on the island of Spiekeroog, Germany, in 1978 (Sengpiel and Meiser 1981) using an early HEM system (DIGHEM II, Fraser 1972) operated by the German Federal Institute for Geosciences and Natural Resources (BGR). Some other authors, e.g., Paterson and Bosschart (1987) and Sengpiel and Fluche (1992), showed examples of the early times of airborne groundwater exploration.

The variety of groundwater related AEM applications is wide. The easiest task is the mapping of saltwater occurrences such as coastal saltwater intrusions (e.g., Fitterman and Deszcz-Pan 1998; Siemon *et al.* 2004; Siemon 2006a), saltwater rises (e.g., Jordan and Siemon 2002) and contaminations (e.g., Smith *et al.* 1992; Paine *et al.* 1997; Siemon *et al.* 2007). Freshwater resources can also be outlined, particularly if a sufficiently strong contrast exists between the freshwater occurrence and the host material (e.g., Christensen *et al.* 2008; Steuer *et al.* 2008a; Viezzoli *et al.* 2008b). Revealing the depth to the aquifer (e.g., Siemon *et al.* 2002), the aquifer thickness (e.g., Smith *et al.* 2004), the aquifer conditions (e.g., Wynn *et al.* 2005), the aquifer recharge conditions (e.g., Cook and Kilty 1992) or the vulnerability of aquifers against pollution (e.g., Röttger *et al.* 2005) are important tasks as well. Airborne EM data is also valuable for delineating special aquifer structures such as fault zones (e.g., Siemon and Greinwald 2004) or buried valleys (e.g., Eberle and Siemon 2006; Christiansen *et al.* 2006). Due to their mapping and sounding facilities AEM data are suitable for 3D modelling, not only for resistivity modelling but also for geological and hydrogeological modelling (e.g., Bakker *et al.* 2006; Rumpel *et al.* 2006; Scheer *et al.* 2006). Recently, airborne EM data have gained increasing importance for salinity mapping, spatial planning and land use management purposes strongly associated with groundwater resources (e.g., Edwards and Macaula 2008; Lawry *et al.* 2008; Munday and Fitzpatrick 2008). A review paper by Paine and Minty (2005) contained further applications and examples on airborne hydrogeophysics.

AEM systems

Today, a variety of AEM systems are used for airborne groundwater investigations. The first AEM system, a Stenmac-McPhar fixed-wing system, was developed in Canada and successfully tested in 1948 for mineral exploration purposes. The principal AEM system geometries using an aircraft or a helicopter as a platform were introduced during the following decade (Fountain 1998). Around the beginning of this century, two types of AEM systems prevailed: rigid-beam helicopter-borne frequency-domain systems and fixed-wing time-domain systems but some new fixed-wing frequency-domain systems and several helicopter-borne time-domain systems have recently been developed (Fountain 2008).

Helicopter-borne frequency-domain electromagnetic (HEM) systems are very suitable for high resolution surveys, particularly if the terrain is too rough for fixed-wing aircrafts. Far more helicopter-borne systems such as GEM-2A, HUMMINGBIRD, IMPULSE, DIGHEM and RESOLVE exist than fixed-wing systems such as HAWK, AEM-05 (Fountain 2008). Helicopter systems use a towed rigid-boom EM system kept about 30–40 m below the helicopter and above ground level. On a fixed-wing frequency-domain electromagnetic (FEM) system, the transmitter and receiver coils are mounted at the wing tips. While a HEM system is towed at a sufficiently long distance below the helicopter, a FEM system has to cope with interactions with the aircraft.

On the other hand, fixed-wing time-domain EM (FTEM) systems are suitable for very large survey areas and great exploration depths. The huge FTEM transmitter coil is slung around the fuselage and wing tips of the aircraft while the small receiver bird is towed several tens of metres below and far behind it. The ground clearance of the FTEM bird is in the order of 60–100 m. Helicopter-borne time-domain (HTEM) systems combine the flexibility of HEM systems and the great investigation depth of FTEM systems but their survey speed is slower and the very near-surface resolution (0–20 m) is generally lower than that of HEM systems. Recently developed helicopter TEM systems are the Aero-TEM, NEWTEM, Hoistem, VTEM, Heli-GEOTEM and SkyTEM systems (Fountain 2008). Most of these HTEM systems were originally designed for mineral exploration. The SkyTEM system, however, has been designed for mapping of geological structures in the near-surface for groundwater and environmental investigations and was developed as a rapid alternative to ground-based measurements.

HEM system design

Modern frequency-domain airborne electromagnetic systems utilize a number of (4–6) small transmitter and receiver coils having a diameter of about half a metre. The primary magnetic field is generated by sinusoidal current flow through a transmitter coil at a discrete frequency. It can be regarded as a field of a magnetic dipole sitting in the centre of the transmitter coil and having an axis perpendicular to the area of the coil. The eddy currents induced in the subsurface by the primary magnetic field generate a secondary magnetic field depending on the conductivity distribution. The secondary magnetic field is picked up by the receiver coil and related to the primary magnetic field expected at the receiver coil. As the secondary field is very small with respect to the primary field, the primary field is generally bucked out and the relative secondary field is measured in parts per million (ppm). Due to the induction process within the earth, there is a small phase shift between the primary and secondary field, i.e., the relative secondary magnetic field is a complex quantity. The orientation of the transmitter coil is horizontal (VMD: vertical magnetic dipole) or vertical (HMD: horizontal magnetic dipole) and the receiver coil is oriented in a maximum coupled position, resulting in horizontal coplanar (HCP), vertical coplanar (VCP) or vertical coaxial coil (VCX) systems. Particularly those systems having several horizontal coplanar coil pairs are suitable for groundwater exploration as the induced currents are predominantly flowing horizontally and thus resolve best layered structures.

HTEM system design

There are several airborne time-domain systems in operation but mainly the new helicopter systems are of interest as they have the sufficient accuracy necessary for groundwater investigations. HTEM systems carry the transmitter loop as a sling load beneath the helicopter. In the transmitter a current is abruptly terminated causing a change of the magnetic field upheld by the current, which in turn causes currents to flow in the ground. Due to ohmic loss the currents diffuse downwards and outwards in the subsurface. The change over time (decay rate) of the secondary magnetic field from these currents is picked up by an induction coil, typically located near the transmitter frame. In most cases both the in-line field (*x*-component) and the vertical field (*z*-component) are picked up by two perpendicular receiver coils. For groundwater purposes the vertical field holds the most important information.

Our paper focuses on a brief introduction to the basic AEM theory as well as on data processing and interpretation tools. Based on field examples using two typical AEM systems, a HEM system (RESOLVE) and a HTEM system (SkyTEM), the advantages and the limitations of AEM groundwater surveys are discussed.

BASIC THEORY

In this chapter we briefly review the basic equations describing the calculation of the field quantities measured by AEM systems as well as inversion methods deriving models for the conductivity distribution in the subsurface.

Frequency domain

Forward calculation

The secondary magnetic field for a stratified subsurface caused by an oscillating (frequency *f*) magnetic dipole source in the air is calculated using well-known formulae (e.g., Wait 1982; Ward and Hohmann 1988). They are based on Maxwell's equations and solve the homogeneous induction equation in the earth for the electromagnetic field vector **f**

$$\frac{\mathrm{d}^2\mathbf{f}}{\mathrm{d}z^2} = \alpha^2\mathbf{f},\ \alpha^2 = \lambda^2 - \omega^2\mu\varepsilon + \mathrm{i}\omega\mu/\rho$$

assuming a homogeneous and isotropic resistivity ρ, which is the reciprocal of the electrical conductivity σ, magnetic permeability μ and dielectric permittivity ε; $\omega = 2\pi f$ is the angular frequency, λ is the wavenumber and $\mathrm{i} = \sqrt{-1}$ is the imaginary unit. The inhomogeneous induction equation containing the source term has to be solved in a quasi non-conductive environment (air) and both solutions are combined at the Earth's surface.

For a horizontal-coplanar coil pair with a coil separation *r* and at an altitude *h* above the surface, the relative secondary magnetic field *Z* is given by (e.g., Ward and Hohmann 1988; Yin and Hodges 2005)

$$Z = r^3\int_0^\infty R_1(f,\lambda,\rho,\mu,\varepsilon)\frac{\lambda^3 \mathrm{e}^{-2\alpha_0 h}}{\alpha_0}\mathrm{J}_0(\lambda r)\,\mathrm{d}\lambda,$$

where $\alpha_0^2 = \lambda^2 - \omega^2\mu_0\varepsilon_0 + \mathrm{i}\omega\mu_0/\rho_0$ with magnetic permeability $\mu_0 = 4\pi \times 10^{-7}$ Vs/Am, dielectric permittivity $\varepsilon_0 = 8.854 \times 10^{-12}$ As/Vm and resistivity $\rho_0 > 10^8$ Ωm of free space, J_0 is the Bessel function of first kind and zero order and R_1 is the complex reflection factor containing the material parameters of the subsurface. This complex integral as well as similar formulae valid for vertical-coplanar or coaxial coil configurations are normally evaluated numerically using fast Hankel transforms (e.g., Johansen and Sørensen 1979; Anderson 1989).

Following the notation of Weidelt (1991) we derive the reflection factor R_1 for an N-layer half-space model by a recurrence formula

$$R_1 = \frac{B_1 - \alpha_0\mu/\mu_0}{B_1 + \alpha_0\mu/\mu_0}$$

with

$$B_\mathrm{n} = \alpha_\mathrm{n}\frac{B_{\mathrm{n}+1} + \alpha_\mathrm{n}\tanh(\alpha_\mathrm{n} t_\mathrm{n})}{\alpha_\mathrm{n} + B_{\mathrm{n}+1}\tanh(\alpha_\mathrm{n} t_\mathrm{n})},\ \mathrm{n} = 1,2,\ldots,\mathrm{N}-1 \text{ and } B_\mathrm{N} = \alpha_\mathrm{N}$$

$$\alpha_\mathrm{n} = \sqrt{\lambda^2 - \omega^2\mu_\mathrm{n}\varepsilon_\mathrm{n} + \mathrm{i}\omega\mu_\mathrm{n}/\rho_\mathrm{n}},\ \mathrm{n} = 1,2,\ldots,\mathrm{N},$$

where ρ_n, μ_n, ε_n and t_n are resistivity, magnetic permeability, dielectric permittivity and thickness of the n^{th} layer, respectively (t_N is assumed to be infinite).

If magnetic effects and displacement currents are neglected (quasi-static approximation), i.e., $\mu = \mu_0$ and $\varepsilon \ll (\rho\omega)^{-1}$, the propagation factors reduce to $\alpha_\mathrm{n}^2 = \lambda^2 + \mathrm{i}\omega\mu_0/\rho_\mathrm{n}$ and particularly $\alpha_0 = \lambda$ in a quasi non-conducting air layer.

In case of lateral resistivity changes, a numerical calculation of the secondary field is necessary (e.g., Newmann and Alumbaugh 1995; Xiong and Tripp 1995; Avdeev *et al.* 1998). Analytical solutions only exist for simple geometries, e.g., a conducting sphere or cylinder. An overview was given by Ward and Hohmann (1988).

Inversion

Generally, the (measured) secondary field data (in-phase and quadrature) are inverted into resistivity using two principal models: the homogeneous half-space and the layered half-space. While the homogeneous half-space inversion generally uses single frequency data, multi-layer (or one-dimensional, 1D) inversion is able to take the data of all frequencies available into account.

The resulting parameter of the half-space inversion is the apparent resistivity (or half-space resistivity) ρ_a, which is the inverse of the apparent conductivity. Due to the skin-effect (high-frequency currents are flowing on top of a perfect conductor) the plane-wave apparent skin depth

$$\delta_\mathrm{a} = \sqrt{\frac{2\rho_\mathrm{a}}{\omega\mu_0}} \approx 503.3\sqrt{\frac{\rho_\mathrm{a}}{f}}$$

increases with decreasing frequency f and increasing half-space resistivity ρ_a. Therefore, the apparent resistivities derived from high-frequency EM data describe the shallower parts of the conducting subsurface and the low-frequency ones the deeper parts.

There are a number of approaches using look-up tables, curve fitting or iterative inversion procedures for calculating HEM apparent resistivities. Comparisons were presented by Beard (2000) and Siemon (2001). As the sensor altitude, which is measured in field surveys by laser or radar altimeters, may be affected by trees or buildings, Fraser (1978) introduced the pseudolayer approach enabling – independent of sensor altitude – the calculation of the apparent resistivity ρ_a and the apparent distance D_a of the HEM system to the top of the conducting half-space. Thus, both data values (in-phase and quadrature or amplitude and phase) have to be used to derive both of the half-space parameters.

The apparent distance D_a can differ from the measured sensor altitude h. The difference of both, the apparent depth $d_a = D_a - h$ is positive in case of a resistive cover (including air); otherwise a conductive cover exists above a more resistive substratum. From the apparent resistivity and the apparent depth the centroid depth $z^* = d_a + \delta_a/2$ is derived (Siemon 2001), which is a measure of the mean penetration of the induced currents.

Half-space parameters obtained for a number of frequencies enable the presentation of HEM results as apparent resistivity maps (Fraser 1978) or apparent resistivity/depth sections (Sengpiel 1983, 1990) or conductivity-depth images (Macnae *et al.* 1998).

There are several procedures for the layered half-space inversion of HEM data available (e.g., Fluche and Sengpiel 1997; Qian *et al.* 1997; Beard and Nyquist 1998; Sengpiel and Siemon 2000; Ahl 2003; Huang and Fraser 2003; Yin and Hodges 2007), which are often adapted from algorithms developed for ground EM data. A comparison was presented by Hodges and Siemon (2008). Many of them use a Marquardt-Levenberg inversion procedure that requires a starting model that should be derived from a resistivity/depth sounding curve (Siemon 2006a).

As the lateral variability of the resistivity is often not very strong in groundwater surveys, particularly for sedimentary aquifers, the model parameters can be tied together by constraints to increase the number of data variables per model and, thus, to enhance both, resolution and stability. Siemon *et al.* (2009), Viezzoli *et al.* (2008b) and Steuer *et al.* (2008b) presented laterally or spatially constrained inversion (LCI/SCI) results for HEM data. We discuss the constrained inversion approach in more detail in the HTEM section.

3D HEM inversion procedures (e.g., Sasaki 2001) are not only scarce but also very intensive in computing time and storage. In practice, 3D modelling is only necessary when strong lateral resistivity changes occur on a local scale. Due to the limited footprint of HEM systems (Beamish 2003), it is mostly adequate to invert the HEM data using a 1D inversion procedure (Sengpiel and Siemon 1998).

Time domain

Forward calculation

As for the frequency domain methods, the time-domain theory is based on solving Maxwell's equations given a set of conditions and assumptions. A detailed description of the theory is found in Ward and Hohmann (1988) and as a shorter version in Christiansen *et al.* (2006).

The vertical magnetic field H_z in the centre of a circular loop, which is a good approximation for a square or otherwise segmented loop of the same area, with radius a and current I, is:

$$H_z = \frac{Ia}{2}\int_0^\infty \left[\mathrm{e}^{-\alpha_0|z+h|} + R_{\mathrm{TE}}\mathrm{e}^{\alpha_0|z-h|} \right] \frac{\lambda^2}{\alpha_0} \mathrm{J}_1(\lambda a)\,\mathrm{d}\lambda$$

with h being the transmitter height and z the receiver height; J_1 is the Bessel function of order one and λ and α_0 as before. R_{TE} is the reflection coefficient and is a quantity expressing how the layered half-space modifies the source field. H_z is expressed in the frequency domain because R_{TE} is a function of frequency (analogue to R_1). The transient response, the response in the time-domain, is obtained by inverse Laplace transform or inverse Fourier transform. The integral is called a Hankel integral. This integral cannot be solved analytically and has to be evaluated using numerical methods.

The expression above applies to the vertical magnetic field in the centre of a circular loop. Any deviation from this setup (piecewise linear loops, off-set loops, x-component of the fields etc.) introduces other equations but, common to them all, only numerical solutions exist. It is very important, no matter the system used, that the system geometry is modelled accurately including frame geometry, frame position (altitude, angle), accurate shape of the transmitted current waveform, timing (to within 0.1 μs) and bandwidths of the receiver system.

However, for visualization purposes there has been a tradition to present data as late-time apparent resistivities using a central loop configuration at the surface of the earth. For this configuration an analytical solution exists for the model of a homogeneous half-space. In this case R_{TE} becomes

$$R_{\mathrm{TE}} = \frac{\lambda - \alpha}{\lambda + \alpha}$$

assuming quasi-static conditions, i.e., $\alpha_0 = \lambda$ and $\alpha = (\lambda^2 + \mathrm{i}\omega\mu_0/\rho)^{1/2}$ and ρ being the half-space resistivity. The vertical magnetic field simplifies to

$$H_z + Ia\int_0^\infty \frac{\lambda^2}{\lambda + \alpha} \mathrm{J}_1(\lambda a)\,\mathrm{d}\lambda.$$

Using the simple relation $\mathbf{b} = \mu_0\,\mathbf{h}$ we can now solve for b_z by evaluating the integral and applying an inverse Laplace transform

$$b_z = \frac{\mu_0 I}{2a}\left[\frac{3}{\sqrt{\pi}\theta a}\mathrm{e}^{-\theta^2 a^2} + \left(1 - \frac{3}{2\theta^2 a^2}\right)\mathrm{erf}(\theta a) \right] \text{ with } \theta = \sqrt{\frac{\mu_0 \sigma}{4t}},$$

where $\sigma = 1/\rho$ is the conductivity of the half-space, t is the time (window) and erf is the error function. b_z may be evaluated for

$t \to 0$ as $b_z = \mu_0 I/2a$. This is the size of the primary field in free space, i.e., the magnetic intensity before the current is turned off.

The decaying secondary magnetic field is referred to as b. As an induction coil is used for measurements in the field, the actual measurement is that of db/dt (the induced electromotoric force is proportional to the time derivative of the magnetic flux passing the coil).

The time derivative, or the impulse response, db_z/dt is found through differentiation to be

$$\frac{\partial b_z}{\partial t} = -\frac{I}{\sigma a^3}\left[3\mathrm{erf}\left(\theta a\right) - \frac{2}{\sqrt{\pi}}\theta a\left(3 + 2\theta^2 a^2\right)\mathrm{e}^{-\theta^2 a^2}\right].$$

When θ approaches zero, i.e., at late times, the time-derivative of the magnetic field can be approximated by

$$\frac{\partial b_z}{\partial t} \approx \frac{M}{20}\left(\frac{\sigma}{\pi}\right)^{3/2}\left(\frac{\mu_0}{t}\right)^{5/2},$$

where $M = I\pi a^2$ is the magnetic moment of the transmitter.

As seen the time derivative of b exhibits decay proportional to $t^{-5/2}$. Observation of the curve of the decaying magnetic field is not very informative and the same applies for actually measured sounding curves. A plot of apparent resistivity ρ_a is more illustrative. It is derived from the late time approximation to be

$$\rho_a = \frac{1}{\pi}\left(\frac{M}{20\partial b_z / \partial t}\right)^{2/3}\left(\frac{\mu_0}{t}\right)^{5/3}.$$

Even though keeping in mind that the apparent resistivity is not equal to the true resistivity for a layered earth, it does provide a valuable normalization of the data with respect to source and the measuring configuration.

These are the central equations for the TEM method but applicable in this form only to the vertical field in the centre of the transmitter loop at the Earth's surface. However, the general behaviour of an airborne system follows that of the equations above and they are often used for data visualization purposes for other configurations as well.

Inversion

Full 3D inversion of TEM data was only very recently presented (Haber *et al.* 2007) and is currently not practically applicable for moving transmitters and receivers. Almost all airborne TEM data are therefore inverted using a 1D layered half-space model.

Within the 1D solution different imaging techniques have so far been the most abundant tools for processing of the data, most of them based on the variation of the diffusion velocity with conductivity, as is the case for frequency-domain methods as well. Nice overviews of these approximate routines can be found in Christensen (2002) and Huang and Rudd (2008).

True inversions using some sort of layered model try to fit the data to a modelled response, minimizing an objective function in a least-squares sense. For ground-based TEM measurements many such true inversion methodologies have been presented and most of these can be used for airborne measurements with only slight modifications. However, true inversion methods are still fairly limited when it comes to airborne TEM methods mainly due to the computational limits implied by the vast amounts of data collected. Examples of inversions schemes for airborne TEM data were presented by e.g., Ellis (1998), Huang and Palacky (1991), Chen and Raiche (1998), Christiansen and Christensen (2003) and Farquharson *et al.* (2003).

In the inversion scheme used for high-quality inversions of SkyTEM data (Viezzoli *et al.* 2008a) the flight altitude is included as an inversion parameter with a prior value and a standard deviation. The inversion of the SkyTEM data is furthermore done using either the 1D laterally constrained inversion developed for inversion of DC data (Auken *et al.* 2005) or the further development of the laterally constrained inversion into the spatially constrained inversion (Viezzoli *et al.* 2008a). In both the laterally constrained inversion and the spatially constrained inversion the model parameters are tied together laterally with a spatially dependent covariance. Constraining the parameters tends to enhance the resolution of resistivities and layer interfaces, which are not well resolved in an independent inversion of the soundings.

The laterally constrained inversion scheme was originally developed for parameterized inversion with normally 4 or 5 layers. Lately, the algorithm has been further developed to include smooth inversion with e.g., 15 layers, each having a fixed thickness but a free resistivity. Both schemes have advantages. Layer interfaces and resistivities are best determined from the parameterized inversion. Also the depth of penetration is better estimated. On the other hand, the smooth inversion is more independent of the starting model and gradual transitions in resistivities are more conspicuous and complicated structures more easily recognizable. Both inversion results can, with advantage, be produced and used together in the final geological interpretation.

DATA PROCESSING

As the reliability of the inversion results strongly depends on the quality of the data used for inversion, not only the hardware capabilities are essential but also the software tools used for data processing. The goal of the data processing is to derive those field values from the data measured that correspond to the subsurface material parameters and to eliminate – or at least minimize – those portions in the data that are affected by influences not belonging to the subsurface.

Frequency domain

HEM data processing requires a number of processing steps such as conversion of measured voltages to relative secondary field values using calibration signals, standard and advanced drift corrections (zero-level drift correction/2D levelling) and – if necessary – data corrections (Valleau 2000; Siemon 2006b). Besides HEM data processing additional parameters like coordinates and altitudes have to be converted and/or corrected. Particularly the altitude data, the distance and the elevation of the system (or the aircraft) to the ground surface recorded by e.g., laser or radar altimeters and GPS receivers (or barometric altimeters), respectively, require thorough processing as they may be affected by system motion and/or reflectors (buildings, trees) above ground level. Particularly, if the altitude is used as an input parameter for the inversion, the effects caused by the tree canopy have to be removed from the altitude data by automatic inspection using a combination of appropriate filters and/or by time intensive manual inspection.

Calibration

The receiver coils of a HEM system measure the induced voltages of the secondary magnetic fields at specific frequencies. These voltages are converted to relative values (in ppm) with respect to the primary fields at the receivers using calibration coils, which produce definite signals in the HEM data measured. As the secondary field is a complex quantity having in-phase and quadrature components, phase and gain adjustment has to take place at the beginning of each survey flight, e.g., using well-defined signals of the calibration coils. Phase and gain adjustments are best performed above highly resistive ground or at high flight altitude. Flight altitudes of several hundred metres (e.g., 350 m for a common HEM system) are sufficient to drop down the signal of the secondary field below the system noise level.

Zero-level drift correction

Remaining signals due to insufficiently bucked-out primary fields, coupling effects with the aircraft or (thermal) system drift are generally detected at high flight altitude several times during a survey flight. These basic values measured at reference points are used to shift the HEM data with respects to their zero levels. This procedure enables the elimination of a long-term, quasi-linear drift; short-term variations caused by e.g., varying air temperatures due to alternating sensor elevations, however, cannot be determined successfully by this procedure.

Therefore, additional reference points – also along the profiles at normal survey flight altitude – may be determined where the secondary fields are small but not negligible. At these locations, the estimated half-space parameters are used to calculate or to check the expected secondary field values, which then serve as local reference levels (Siemon 2009).

2D levelling

Standard airborne surveys consist of a number of parallel profile lines covering the entire survey area. Thus, statistical methods and/or 2D filter techniques called statistical levelling (tie-line levelling) and empirical levelling (micro-levelling), respectively, are applicable to correct stripe patterns in airborne geophysical data sets (e.g., Huang 2008). Standard levelling procedures developed for e.g., airborne magnetic data, are, in general, not directly applicable to HEM data, because HEM data levelling faces the problem that the parameter affected by zero-level errors, the secondary field, differs from the parameter generally levelled, the apparent resistivity (Huang and Fraser 1999). Furthermore, the dependency of the secondary field on both the resistivity of the subsurface and the sensor altitude is strongly non-linear. Therefore, the half-space parameters apparent resistivity and apparent depth, followed by a recalculation of the secondary field components based on the half-space parameters levelled, should be used for HEM data levelling (Siemon 2009).

Data corrections

Noise from external sources (e.g., from radio transmitters or power lines) should be eliminated from the HEM data by appropriate filtering or interpolation procedures. Induction effects from buildings and other electrical installations or effects from strongly magnetized sources should not be erased from the data during the first step of data processing. These effects appear particularly on a low-frequency resistivity map as conductive or resistive features outlining the locations of man-made installations or strongly magnetized sources, respectively. If necessary, these effects can be cancelled out after a thorough inspection and the data may be interpolated in case of small data gaps and smoothly varying resistivities. If attitude data (pitch and roll) are available, HEM (and altitude) data can also be corrected for system movements (e.g., Fitterman and Yin 2004; Yin and Fraser 2004; Davis *et al.* 2006).

Time domain

HTEM data processing is performed on many different levels, depending on the target of the survey. In groundwater exploration, data with precision and quality are required as the decisive data changes can be as low as 10–15%. When operating in the air a number of key issues need to be addressed to achieve the required data quality. Different processing schemes exist for different systems. This overview is based on the scheme used for high-quality SkyTEM data processing (Auken *et al.* 2007) but the main issues apply to most HTEM systems if used for groundwater purposes.

Full SkyTEM data processing is generally a four-step process. Step 1 is processing of navigation data (GPS, altitude and tilt measurements). The navigation data are filtered and averaged automatically but manual corrections may have to be applied to the altitude data. Step 2 is processing of the voltage data. This step is also automatic and includes filtering and averaging. Standard deviations based on the data stacks are also calculated here. In step 3 the voltage data are evaluated manually for further refinement of the processing (necessary in areas with infrastructure). Finally, in step 4 a fast inversion using a smooth model is used to fine-tune the processing done in step one to three.

Calibration

When airborne systems are operating in the time domain, contrary to the frequency domain, it is possible to reduce the interaction between the transmitter and the receiver system to a level, at which the distortion of the measured off-time signals is negligible. In this case, a calibration of the instruments can be performed in the laboratory and/or at a test site before the equipment is used in surveys. Neither high altitude measurements nor performing tie lines for levelling are then necessary during the survey. The SkyTEM system and perhaps one or two other HTEM systems are in this sense absolutely calibrated. In production, the system is verified to a ground-based measurement before the first flight. On any further take-offs and landings a measurement at 10 m elevation is repeated and reproduction ensured.

Navigation data processing

As mentioned above navigation data are filtered and averaged automatically and manual corrections are applied to the altitude data if needed. The result of the automatic processing is inspected using profile plots of flight time versus data value (tilt, altitude, voltage data, etc.). The plot also shows various quality control parameters; for example flight speed, topography, tilt (both pitch and roll), transmitter temperature, etc. A key feature in the processing is using an integrated interactive GIS map where the helicopter location is highlighted. Combined with proper GIS themes it is possible to explain most features in the data; for example that the sudden increase in altitude and somewhat coherent noise is an effect of the helicopter crossing a power line, that the lasers get bad reflections because the helicopter is flying over a forest, etc.

The tilt is measured both in front of the frame and at the back of the frame. The tilt measurements are important for the correction of the altitude measurements and as input to the inversion when inverting both x- and z-component data.

The altitudes of the transmitter frame and receiver coils are measured using two laser altimeters at different positions at the frame. Most problems with determining the correct altitude using lasers are caused by the laser beam not being reflected from the surface of the ground but by leaves. To eliminate these erroneous reflections and correct for the laser beam not always being vertical several corrections steps are taken. Firstly, the altitude has to be calculated at the centre of the transmitter frame, secondly the altitudes are recursively filtered to remove treetop reflections and thirdly they are averaged and the altitudes of the receiver coils are calculated.

Processing of voltage data

The raw voltage data are collected with a certain number of transients in the stack. The number of transients in the stack is set so that the desired signal-to-noise ratio is obtained and, equally important, the power-line frequency (and its most powerful harmonics) is stacked out.

In the system measuring cycle the natural background level is also included. This is simply done by turning off the transmitter while the system still runs. The noise measurements are typically done for each 40th or 60th normal measurement.

Data from areas with a significant amount of infrastructure such as pipes, power lines and metal fences unfortunately require a significant amount of manual processing even though filters have been designed to help cull disturbed data. These data are removed entirely from the raw stacks as they will otherwise be smeared out and significantly degrade the quality of the data that are not influenced by couplings. Danielsen *et al.* (2003) discussed the physics behind the galvanic and capacitive coupling phenomena. Designing filters to detect galvanic couplings is next to impossible as the signal level is just raised and does not show oscillation as does the capacitive coupling. The capacitive coupling detection filter works by examining both the raw data stacks for undesired curve slopes and the sign changes within the time interval where one can expect useful signal.

Typically all data at a distance of 100–150 m from roads, power lines, wind mills, slurry tanks etc. need to be culled. The exact distance is dependent on the subsurface conductivity, a low conductive ground produces a low electromagnetic response that increases this distance, while a highly conductive ground produces a large signal and the coupling distance is decreased.

An optimal data-averaging scheme

Traditional data averaging uses a ‘square’ averaging core if seen on a gate-time versus flight-time (or distance) scale, i.e., data are averaged over the same length of time (equal to distance) at early times as at late times. This approach has a downside that it is not possible to maintain a high resolution at early times (corresponding to the near-surface), where the signal-to-noise ratio is usually relatively high, while still obtaining a reasonable signal-to-noise ratio at late times, i.e., a large penetration depth. Furthermore, in quasi-layered environments it must be stressed that having a small sounding distance, e.g., 5 m, does not necessarily correspond to a high lateral resolution if data are still averaged over large time spans/distances, e.g., 150 m. It just means a high level of redundant information.

We use instead trapezoid formed average cores so that early time data are averaged less than late time data. This approach is actually an image of the nature of the electrical fields in the substratum itself. Doing this, we a) maintain the optimal resolution of the near-surface resistivity structures and b) obtain a reasonable signal-to-noise ratio at late times, thereby maintaining the desired penetration depth.

Smooth inversion for post processing of voltage data

We find it useful to run a smooth inversion of the average data as the final step in the processing. We use the laterally constrained inversion algorithm (Auken *et al.* 2005) because constraining the model parameters laterally works well even if the data are noisy. This inversion is used to remove outlier data, which for some reason have not been removed in the automatic filters or manual processing.

CASE HISTORIES

From the long list of possible applications of AEM surveys in groundwater exploration we selected two case histories not published before. In the first case history from a German island an airborne frequency-domain system (Fig. 1) is used to successfully locate freshwater lenses on top of saltwater. The second example from Denmark shows how a time-domain system is used to locate large-scale buried structures forming ideal groundwater aquifers.

HEM survey of Borkum, NW Germany

Survey area

The island of Borkum, Germany, is the largest (31 km^2) and westernmost of the East Frisian Islands in the North Sea. It is bordered to the south-west by the Western Ems strait close to the border to The Netherlands, to the north-east by the Eastern Ems strait, to the north-west by the North Sea and to the south-east by the mouth of the river Ems. Borkum belongs to the barrier islands whose origin and development have been influenced by waves and tides. As a geologically recent landscape (about 3000 years old), Borkum as well as the other East Frisian Islands are characterized by Quaternary deposits, mainly sand, silt and clay. The landscape is dominated by dunes, particularly along the north coast, grassland and salt marches.

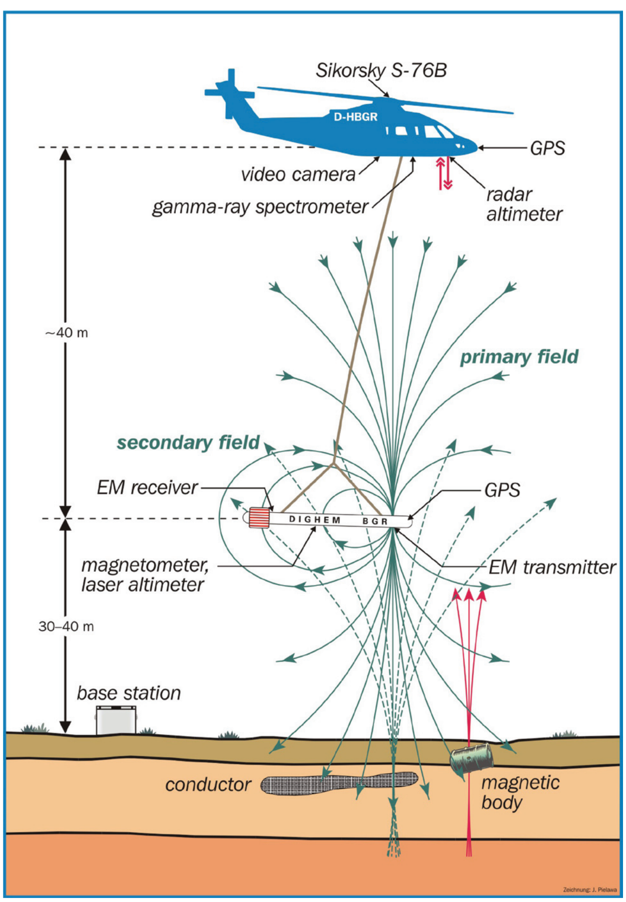

FIGURE 1
BGR's helicopter geophysical system.

Hydrogeological situation

Until the mid of the 18th century Borkum consisted of two islands, Ostland and Westland, separated by a tidal creek. Each of them had their own freshwater lens being recharged by rain only. Due to installation of barriers both islands merged together but the freshwater lenses are still separated.

As the growing tourism industry is the most important income source of the island, the annual water consumption has risen dramatically during the last decades, particularly in summer times. In order to satisfy the demand of fresh and service water, the shallow (less than 12 m) groundwater well network was extended from Westland, where the village Borkum is located, to Ostland. There, however, some of the shallow water wells had to be closed because of the poor chemical water conditions; particularly the water contained a great amount of organics due to humus layers between 4–12 m depth. Geophysical measurements (DC geoelectrics) conducted in 1972 revealed an up to 60 m thick freshwater lens in Ostland being thickest where no clayey cover exists (Gerhardy 1975).

The storm surge of the winter 2006/2007 damaged the island of Borkum considerably. On Ostland heavy losses of protective dunes occurred along the north-east coast enabling a seawater flooding that reached the freshwater well catchment areas. In order to estimate potential future damages on the freshwater catchment area detailed investigations revealing the spatial extent of the freshwater lenses, their volume and water content were necessary.

Airborne survey

Initiated by local waterworks BGR and the Leibniz Institute for Applied Geophysics (LIAG, formerly GGA Institute) conducted airborne and ground-based geophysical measurements in March 2008. The airborne survey covered an area of about 80 km^2 (Fig. 2). The 35 NW-SE lines and 11 SW-NE tie lines totalling 420 line-km were flown within two days with four survey flights commencing from the airport Emden about 30 km south-east of the survey area. The line spacing was 250 m and 500 m for the lines and tie lines, respectively. The tie-line spacing was chosen rather low in order to get a net-like coverage of the island with lines running as perpendicular as possible to all coast lines.

The BGR helicopter system (Fig. 1) measures simultaneously electromagnetic, magnetic, radiometric and position data at a sampling rate of 10 Hz (radiometrics: 1 Hz). Having a survey speed of about 150 km/h the sampling distance is about 4 m (radiometrics: 40 m). The HEM system (RESOLVE, Fugro Airborne Surveys) operates at six frequencies ranging from 386 Hz to 133 kHz. The coil separations of the five HCP and one VCX coils are about 7.9 m and 9.1 m, respectively.

As all flights were also flown over the North Sea, the deeper (more than 10 m) seawater flight sections could be used to check the calibration of the HEM data. Assuming a constant conductivity of seawater the HEM data were tuned to a common apparent resistivity of 0.2 Ωm and an apparent distance equalling the sensor height measured by the laser altimeter.

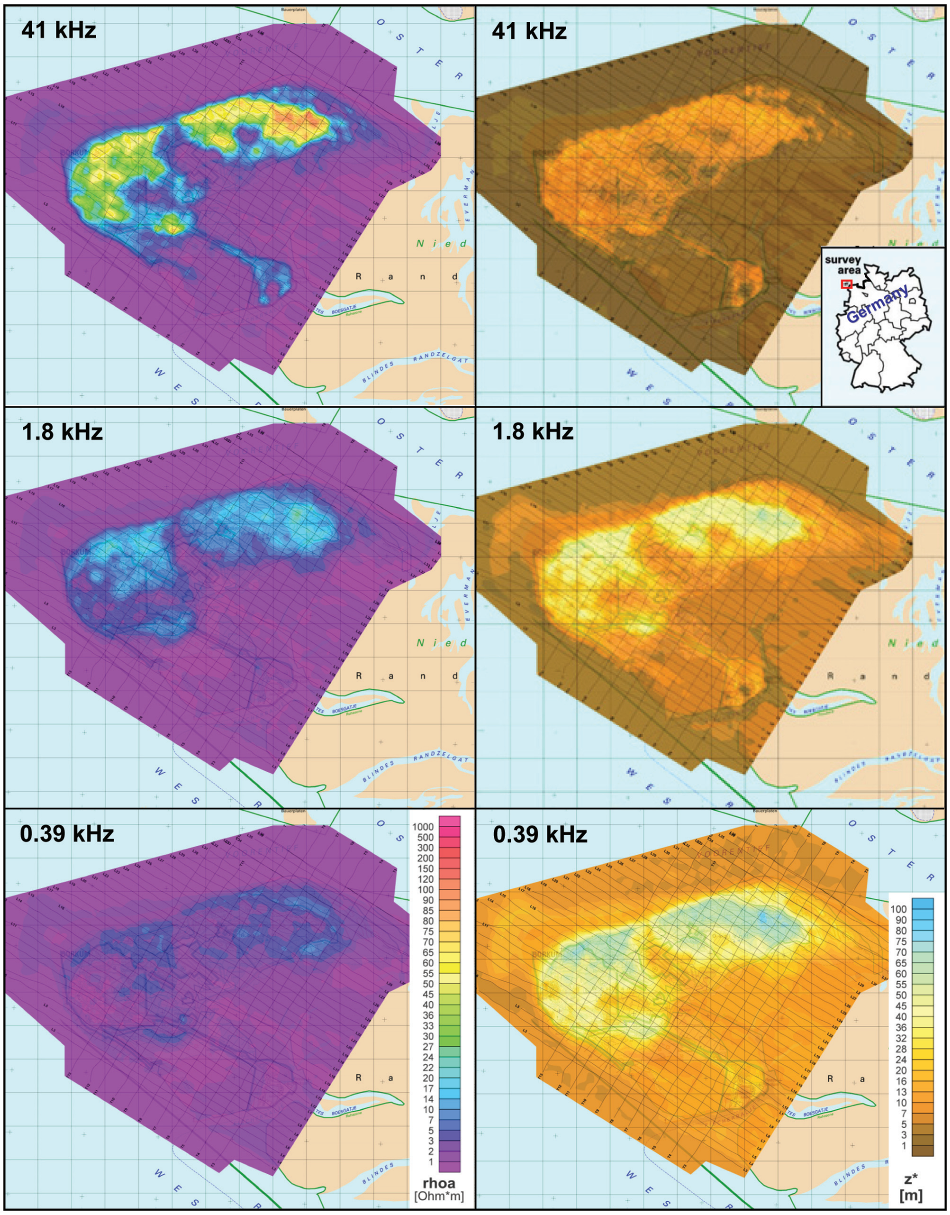

FIGURE 2
Apparent resistivity maps (left) and centroid depth maps (right) covering the island of Borkum in NW Germany (see inlet map) for three frequencies (41 kHz, 1.8 kHz and 0.39 kHz). The violet, dark blue, light blue and green to orange colours on the apparent resistivity maps represent seawater, saltwater saturated sediments, brackish water or clayey sediments and freshwater saturated sands, respectively. The corresponding centroid depth maps show the increasing depth of penetration from high to low frequencies. Both types of maps clearly outline two freshwater lenses, on Westland (left one) and Ostland (right one). The net of flight lines is indicated by thin black lines.

Results

Apparent resistivity and centroid depth maps were produced for all frequencies. A selection of these maps (Fig. 2) clearly shows that:

- the freshwater resource of the island of Borkum consists of two freshwater lenses (green to orange colours, $\rho_a > 30\ \Omega$m);
- the EM fields of the lowest frequency penetrate the entire freshwater body and reach the saltwater saturated sediments below (violet colours, $\rho_a < 3\ \Omega$m);
- the thickest freshwater layers having centroid depth values of about 60 m (light green colours) are located in the northern parts of both Westland and Ostland.

Although maps of apparent resistivities and centroid depths clearly outline the lateral extent of resistivity structures like freshwater lenses, they are less accurate on the vertical scale. Therefore, 1D inversion models were derived from the HCP data for each of the reading points (>100,000) using both single-site and laterally constrained Marquardt-Levenberg inversion procedures (Siemon *et al.* 2009). The five-frequency data were inverted into the parameters of a four-layer model. The first layer is necessary to represent the sediments above the water table. Thus, this layer is highly resistive and rather thin, particularly where no dunes exist. The fourth layer clearly represents the saltwater saturated sediments below the freshwater lenses. The area between these two boundary layers is subdivided in another two layers, one representing the freshwater saturated sands and the other is necessary to model brackish water or clayey sediments. This rather simple model, however, is not suitable for

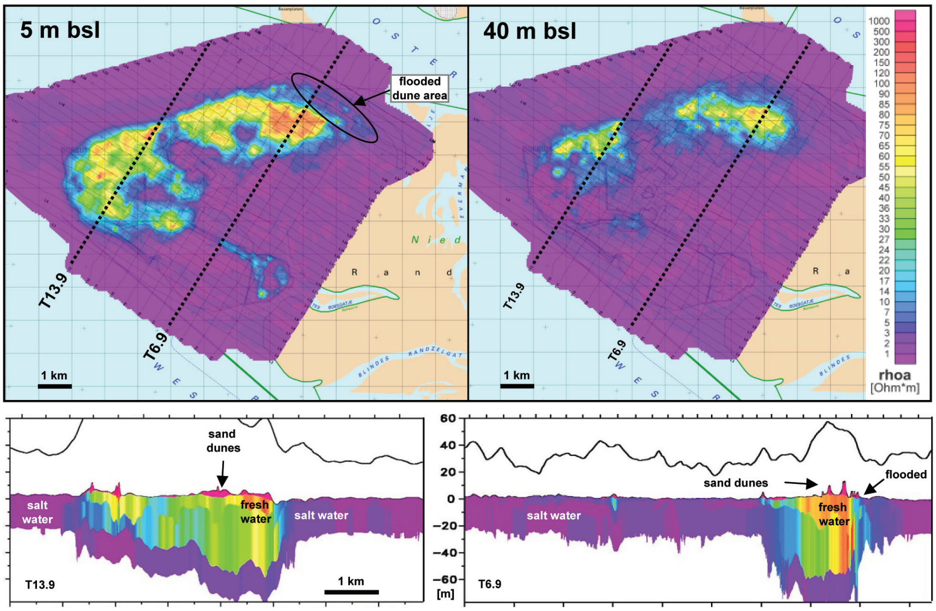

FIGURE 3
1D inversion results: resistivity maps at 5 m and 40 m bsl (above) and resistivity cross-sections along tie lines T13.9 and T6.9 (below) crossing Westland and Ostland, respectively (dotted lines on the maps).

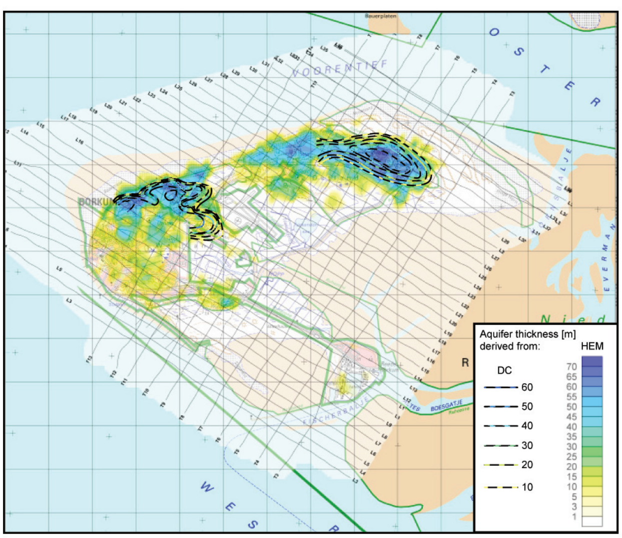

FIGURE 4
Freshwater aquifer thickness map based on recent HEM (colours) and old DC (lines) measurements.

resolving complex layering such as a clay layer sandwiched between freshwater saturated sand layers. Off-shore, the model layers represent seawater or seawater saturated sediments, i.e., in deep-water areas all layers should be very similar in their resistivity corresponding to that of seawater.

From the resistivity-depth models resistivity cross-sections along all survey lines and resistivity slices at certain depths were derived. Examples are shown in Fig. 3. The two resistivity sections (tie lines T13.9 and T6.9) cross the freshwater lenses of Westland and Ostland, respectively.

The eastern part of T6.9 also crosses an area that has been flooded due to heavy storms. From the resistivity section it can be concluded that this seawater flooding has not significantly affected the freshwater lens on Ostland.

The inversion results also demonstrate that both the lateral and vertical extent of the freshwater lenses could be outlined completely. Therefore, these results are suitable to derive the thickness of the freshwater aquifers. Assuming that water can be expected as fresh when the water conductivity is lower than 180 mS/m (cf., Paine and Minty 2005), i.e., the water resistivity should be higher than 5.6 Ωm and that an overall formation factor of $F = 4$ represents the sediments of the island of Borkum (Gerhardy 1975), the bulk resistivity of freshwater saturated sediments should be higher than

$$\rho = F\rho_w = 4 \times 5.6\ \Omega\text{m} = 22.2\ \Omega\text{m}.$$

Accumulating all layer thicknesses having resistivities between 30–500 Ωm leads to aquifer thicknesses, which are shown in Fig. 4. These results agree reasonably well with DC geoelectric results obtained on Ostland (Worzyk 1995a) and Westland (Worzyk 1995b) in 1991–1994.

The HEM data set was also used to estimate the volume of freshwater available on the island of Borkum. Pignon (2008) tested several software packages for volume estimations. One of them is Geosoft Oasis montaj that uses the 3D Kriging method to create a 3D voxel model. Due to the huge number of voxels necessary for creating a high resolution model of the entire survey area, Pignon decided to build a rough voxel model consisting of 70 m × 70 m × 20 m voxels. Using a threshold value of 50 Ωm, 9021 voxels characterize the volume of the freshwater lenses resulting in a total volume of 884 × 10^6 m^3. Another very simple approach is to accumulate the aquifer-thickness values, which are greater than a minimum value of 1 m (Fig. 4) and multiply these values by the grid size used (50 m × 50 m) in

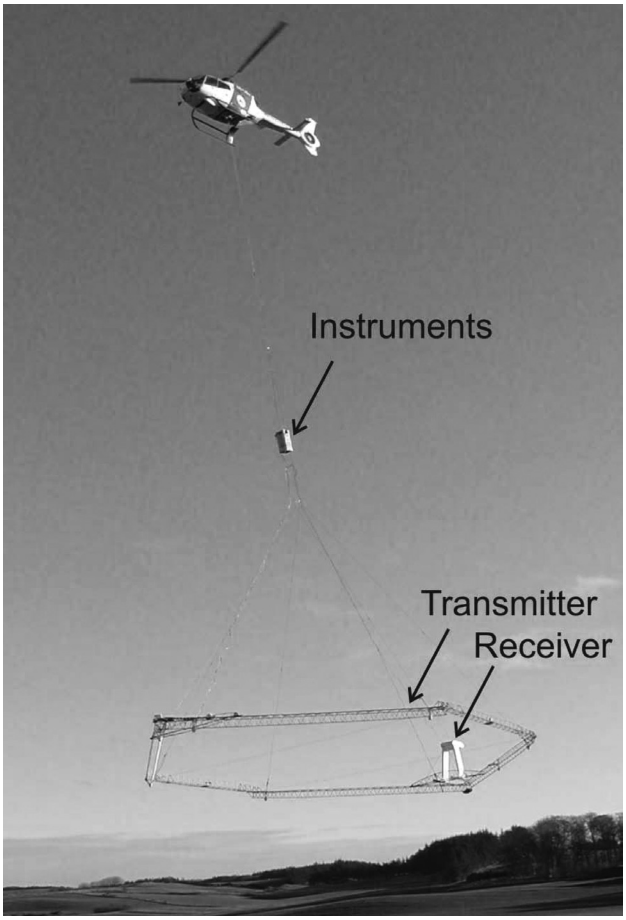

FIGURE 5
The SkyTEM system in operation.

order to derive the total volume of freshwater saturated sediments. Although the volume derived by this method (525×10^6 m^3) is smaller than the volume received by 3D gridding, this result seems to be more realistic as the resolution is definitely better, particularly in vertical direction. Assuming a porosity of about 33%, what corresponds to a formation factor of $F = 4$ for sandy aquifers (Kirsch 2006), the total water content can be approximately estimated to be of the order of 175×10^6 m^3.

SkyTEM survey, North Jutland, Denmark

Survey area

Over the past few years, the helicopter-borne SkyTEM system (Fig. 5) has collected many thousands of kilometres of TEM data, many of them in sedimentary environments for groundwater exploration. In the following we will show results from a large survey in the northern part of the Jutland peninsula, Denmark. A subsection of the full survey is seen in Fig. 6. The red dots are SkyTEM soundings, the blue dots are ground-based measurements conducted prior to the airborne campaign. The red dot on the insert indicates the survey location in the northern part of Jutland.

Hydrogeological situation

In the last decade the county of Northern Jutland has carried out large hydrogeological surveys in Vendsyssel, Northern Jutland. The purpose of each of these mapping campaigns has been to locate deep lying aquifers as replacements for more shallow aquifers. In a regional plan from 1997 areas with special drinking water interests were selected based primarily on existing borehole information. The general strategy for aquifer structure and aquifer vulnerability surveys is to locate deep-lying aquifers

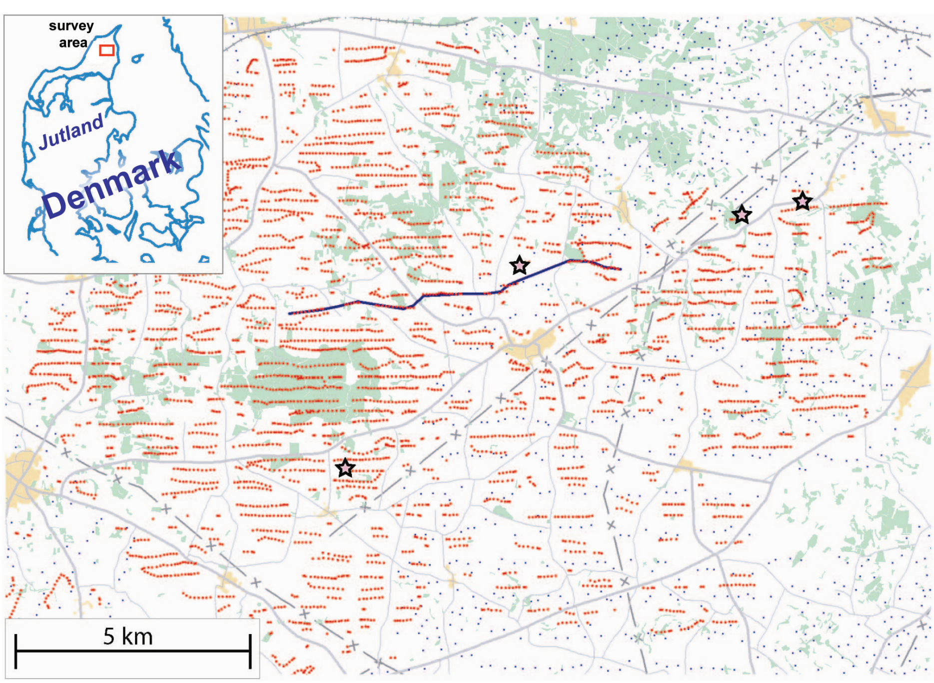

FIGURE 6
The map shows the location of the survey of the northernmost part of Jutland, Denmark (see inlet map). The red dots mark the soundings from two SkyTEM surveys and the blue dots mark ground-based soundings. The solid grey lines are roads and the dashed grey lines are the power lines. The blue line is the profile shown in Fig. 9. The stars indicate the positions of boreholes drilled after evaluation of the SkyTEM survey.

covered with clay layers. Consequently, the areas were primarily selected where the drill holes proved the existence of protective shallow clay layers. The surveys carried out until 2003–2004 have unfortunately in most cases revealed clay layers of a thickness that prevents seepage of groundwater and extraction of water below them. In other cases, aquifers with low quality groundwater or too low hydraulic permeability were located. The strategy then changed so that the drinking water interest areas are selected where the water has a sufficient quality and quantity even with incomplete natural protection. The consequence of this change is that the groundwater protection must be active and if necessary land must be left unexploited or restrictions put on the use. In addition, larger waterworks in the area can be forced to divide their extraction sites into smaller and more decentralized sites. The waterworks in the larger cities of the area have the most urgent problems with limited water resources. Some extraction sites show organic solvents and pesticides and poor natural water quality in general.

The geology in the Vendsyssel area can be generally described by a surface of clay deposited in seawater overlain by sediments deposited in freshwater during the last glaciations and tills. The upper-most sediments consist of seawater deposited sand and clay layers. The different surveys have shown that, in general, groundwater cannot be extracted from depths larger than about 80 m – not only because of the bottom clay layer but also because of residual saltwater. Many of the potential aquifers consist of fine grained deposits with a low hydraulic permeability. The deposits originate from a large meltwater lake located centrally in the area. The near-surface geology is disturbed with pushed up clay sheets and buried valleys.

After the change in strategy, the HydroGeophysics Group (HGG) at the University of Aarhus was invited to participate in a consortium together with the county and a private consulting company. The aim of the consortium was to build a preliminary geological model and based on that model to map an area of more than 300 km^2 with SkyTEM.

The SkyTEM system

The SkyTEM system (Fig. 5) has been developed for groundwater investigations by the HGG group at the University of Aarhus, Denmark (Sørensen and Auken 2004). The system has been intensively used for groundwater surveys. The transmitter and receiver coils, power supplies, laser altimeters, global positioning system (GPS), electronics and data logger are carried as a sling load on the cargo hook of the helicopter.

The frame is located using two GPS position devices. The altitude is measured using two laser altimeters mounted on the carrier frame, as well as inclinometers measuring in both the *x*- and *y*-directions. The measured data are averaged, reduced to data subsets (soundings) and stored together with GPS coordinates, altitude and inclination of the transmitter/receiver coils and transmitter waveform. Transmitter waveform information and other controlling parameters of the acquisition process are recorded for each data subset, thereby ensuring high data-quality control.

The transmitter loop for this survey was a four-turn 300 m^2 loop divided into two segments allowing transmittance of a low and a high moment. The transmitter loop is attached to a rigid wooden lattice frame construction. The receiver coil is located on the rudder, 1.5 m above the corner of the transmitter loop as shown in Fig. 5.

The operational flying speed of the SkyTEM system in groundwater surveys is nowadays approximately 45 km per hour but this particular survey was flown at approximately 20 km per hour providing a high-moment stack size of approximately 1000 transients. Consequently, high- and low-moment data segments yield an average lateral spacing of 35–45 m. A compromise between vertical resolution and safety concerns for the helicopter operation is to maintain an altitude of 15–20 m for the carrier frame.

Processing and inversion

A sounding consists of a low and a high-moment segment. As the two segments are spatially separated, the data sequences are inverted with different altitudes. The flying altitude is included as an inversion parameter with a prior value and a standard deviation determined from the altimeters. All data sequences along the profile lines are inverted in one step using soft bands on the model parameters. This laterally constrained inversion approach allows for smooth transitions along the profile line resembling the actual changes in geology.

The forward modelling of the transient data is independent of the chosen inversion scheme. We do not deconvolve the system transfer function from the field data as in our experience deconvolution is an inherently unstable process. The transmitter waveform is applied using a piecewise linear approximation to the current waveform and the low-pass filters are applied following Effersø *et al.* (1999). Filters before the front gate (a gate preventing the primary field from the current turn-off to saturate the amplifiers) are calculated in the frequency domain while filters after the front gate are calculated by a convolution in the time-domain.

Results

Figure 6 shows a map of the northernmost part of the SkyTEM survey that we will focus on here. An impression of the flight paths is given by observing the red dots showing the SkyTEM sounding points. Data are absent along roads, power lines and windmills due to capacitive or galvanic couplings because of transmitter-induced couplings to the power lines and other cables (Danielsen *et al.* 2003). The whole survey comprises 1250 line kilometres of SkyTEM data or more than 9000 individual soundings.

The first thematic map we present is the depth to a low resistive layer derived from 1D inversion models, see Fig. 7. This layer is interpreted as being identical to the marine clay that also outlines the bottom of any potential aquifer in the area. As seen, the area is characterized by a relatively flat lying clay surface incised by relatively narrow buried valley structures. The most

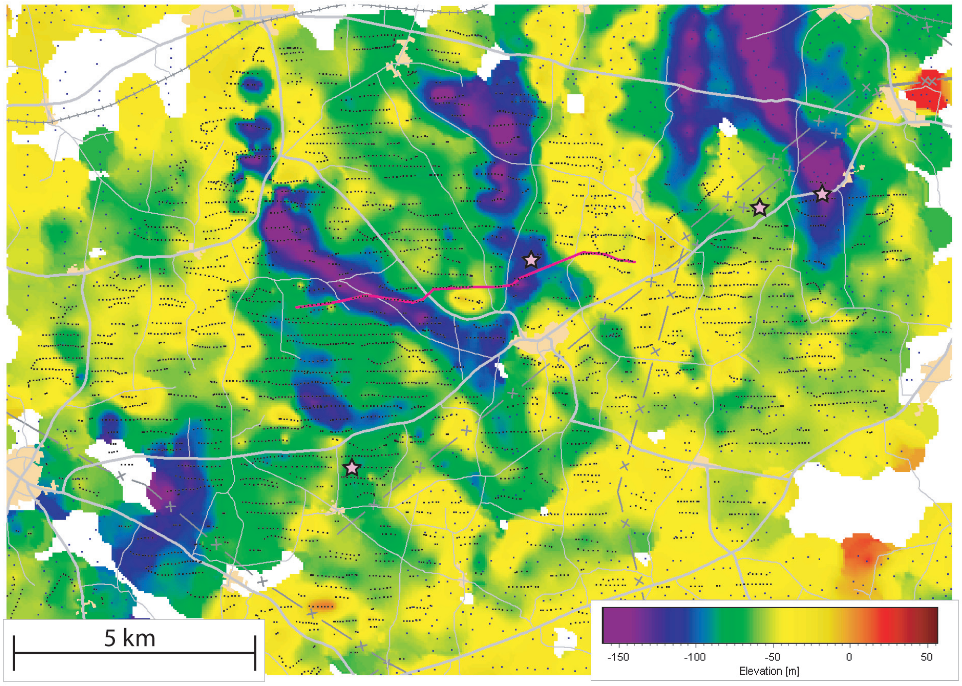

FIGURE 7
The map shows the elevation of the good conductor (<10 Ωm). The red line is the profile shown in Fig. 9. The map is based on both the SkyTEM models and models from previous ground-based surveys (the scattered points in the NW, NE and SE corners). The stars indicate the positions of boreholes drilled after evaluation of the SkyTEM survey.

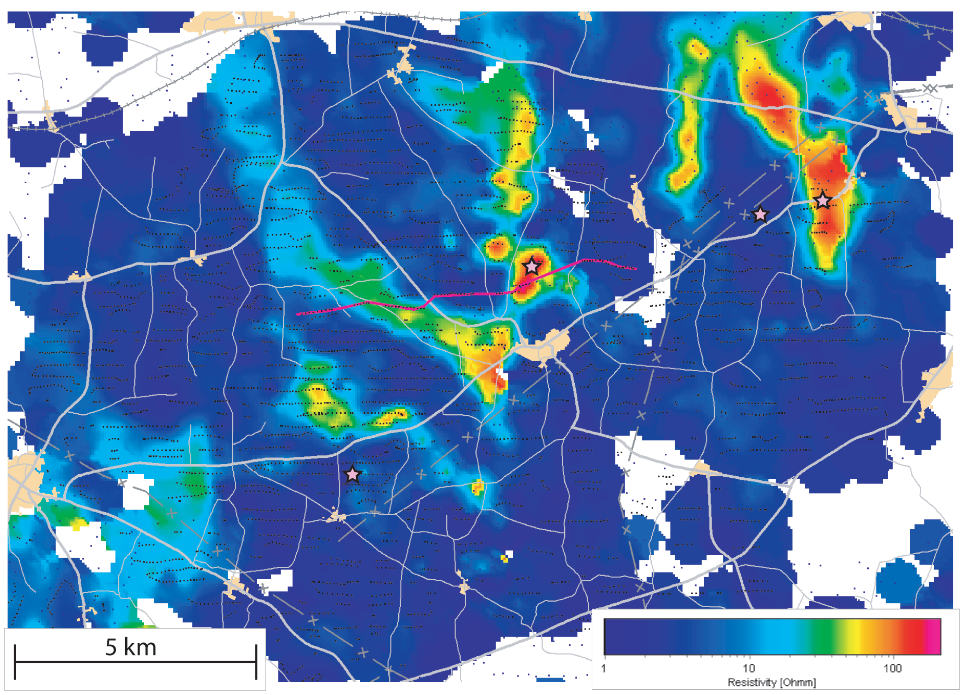

FIGURE 8
The map shows the average resistivity in an interval from 80–90 m below sea level. The red line is the profile shown in Fig. 9. The map is based on both SkyTEM models and models from ground-based soundings. The stars indicate the positions of boreholes drilled after evaluation of the SkyTEM survey.

pronounced buried valleys are incised more than 100 m into the clay. Buried valleys are very common in Denmark (Jørgensen *et al.* 2003a,b) and often they are an important groundwater resource, particularly if a course-grained valley fill is protected by a clayey cover.

It must be emphasized that the buried valley structures in the central part of the survey area were not known prior to the SkyTEM survey. The structures are not visible in the landscape, which, as a matter of fact, forms an up to 90 m high ridge.

Evaluation of the resistivity of the fill in the buried valleys is done on thematic maps showing the average resistivity in different elevation intervals. More detailed studies can be made on cross-sections. An example of an average resistivity map is shown in Fig. 8.

The map shows the average resistivity of the subsurface in the interval from 80–90 m below sea level and several buried valley

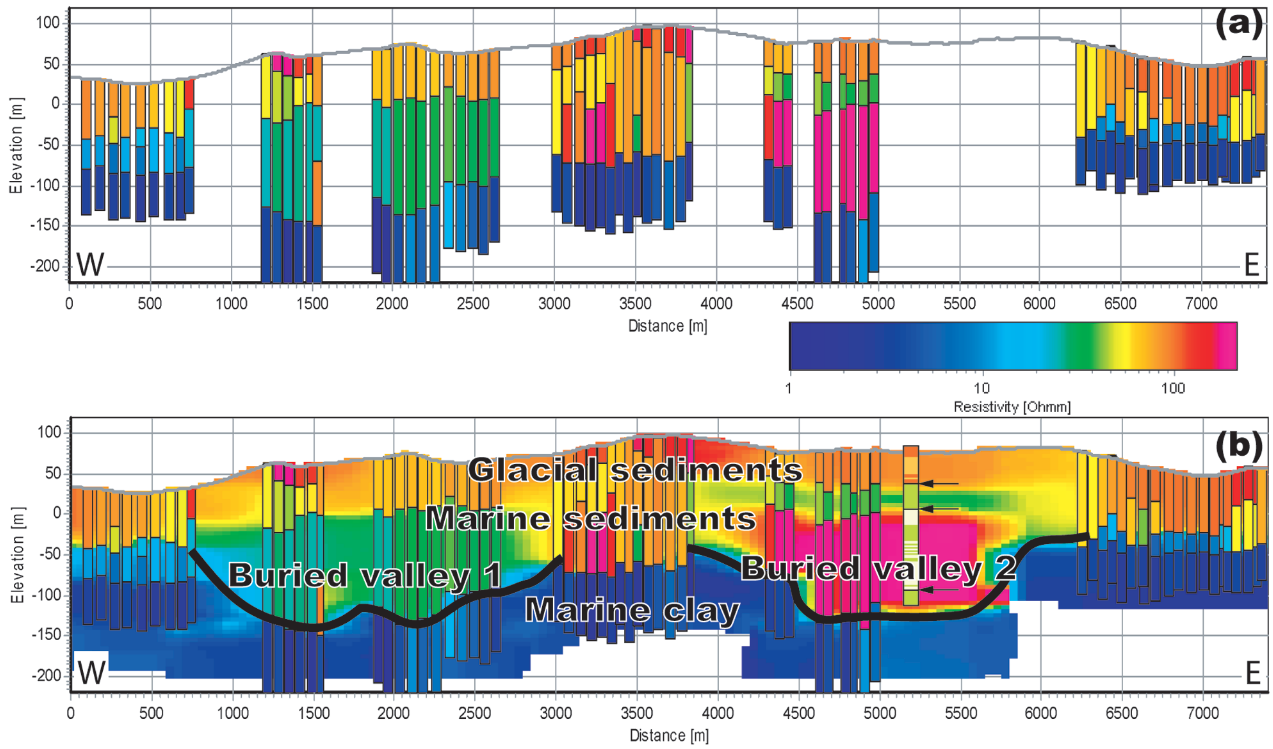

FIGURE 9

W-E profile in the survey area as shown on the area maps. The coloured bars show the 1D models projected onto the profile line. In a) only the SkyTEM models close to the profile are shown. In b) these model bars are drawn on top of a cut through a stack of average resistivity maps to give an impression of the structures for the entire section. Also on b) a rough geological interpretation is shown together with the nearest borehole (for location see Fig. 6). The borehole shows lithological information. Orange colours are quaternary sands, green and cream colours are tertiary silts, clays and sands. For simplicity the three main boundaries are indicated with arrows. The borehole is 300 m away from the profile line.

structures trending N-S and NW-SE are seen. If we interpret blue and green colours (< 40 Ωm) as clay or clay dominated sediments and yellow and red colours (> 40 Ωm) as sand and gravel dominated sediments, it is obvious that some of the buried valley structures are in fact filled with sand and gravel and are therefore potential aquifers. Other valleys, as the one in the west-central part of the area, cut by the profile line, is very clear in the elevation map in Fig. 7 but on the average resistivity map it is seen that the fill sediments have resistivities around or below 20–30 Ωm (green) for large parts of the northern end. Therefore, it has no interest in a hydrological context. Numerous buried valleys originating from various ice progressions from different directions are clearly visible on the average resistivity maps when inspecting and comparing maps from other elevation intervals (not shown here).

Figure 9(a) shows the profile drawn on Figs 6–8 as a section where the geophysical models are shown as bars. In Fig. 9(b) a cut through a stack of average resistivity maps are draped along the section to give a full impression of the resistivities. The surface of the bottom clay layer has two distinct lows, which are the buried valleys mentioned earlier. A simple geological interpretation is drawn on top of the sections. The valley termed 'Buried Valley 1' has an infill of sediments with resistivities around 20–30 Ωm, which are, as already mentioned, hydrogeologically not very interesting. The 'Buried Valley 2', though, has very promising infill of more than 100 Ωm suggesting freshwater saturated sands. In addition, there is a protective clay layer on top of the potential aquifer, which is very important for the protection of the aquifer to pollutants.

Based on the SkyTEM survey and on the first geological model of the area it was decided in the spring of 2005 to drill five deep investigation drillings in the northern part of the area and another four drillings in the winter of 2005/2006. The boreholes were primarily located in the incised valleys filled with highly resistive sediments, as seen in Figs 6–8 (not all of the new drill-holes fall within the depicted area). However, in order to get information about the entire stratigraphy two drillings have been sunk outside the valleys.

All the first five drillings have confirmed the existence of the buried valley structures. They have also confirmed that coarse sandy sediments exist in some of these valleys and water samples have shown a reasonable water quality. Hydraulic measurements have not been made yet but the grain size from the geological samples indicates that the hydraulic conductivity of the formation is acceptable. One of these drillings is 300 m away from the section shown in Fig. 9 and is projected onto the section as well. The major boundaries coincide nicely with the general resistivity structures. The depth to the bottom of the valley seems to be underestimated but given the distance from the drillhole to the profile (300 m) compared to the size of the valley this is fully acceptable.

DISCUSSION AND CONCLUSIONS

Airborne electromagnetics is a very useful method for surveying large areas in order to support hydrogeological investigations. Due to the dependency of the geophysical parameter electrical conductivity on water content, water chemistry, pore volume and structure and the electrical properties of the host mineral grains (McNeill 1980), information about water quality and aquifer characteristics can be derived from AEM data. The results, however, are sometimes ambiguous: a clayey aquitard in a freshwater environment and a brackish, sandy aquifer, for example, are associated with similar conductivities. As a consequence, additional information, e.g., from drillings, are required for a solid hydrogeological interpretation of the AEM data.

Airborne electromagnetic surveys increasingly gain importance in groundwater exploration. Particularly in large-scale (> some 10 km^2) surveys they are indispensable due to technical and economical reasons. Even at medium-scale (< some 10 km^2) airborne systems may be more suitable for groundwater surveys than measurements on ground, e.g., in hardly accessible areas. Compared to ground geophysical measurements AEM measurements are definitely faster, cover larger areas, provide generally a higher spatial density and are nearly everywhere applicable. On the other hand AEM measurements cannot reach the resolution capabilities of ground and borehole EM systems as the distance of the AEM system to the region of interest is, of course, greater and thus, the system footprint is larger.

Frequency-domain electromagnetic measurements are suitable for high-resolution surveys as long as the targets are seated not deeper than 100 m. For deeper targets ground-based or airborne time-domain measurements are more suitable. Helicopter-borne multi-frequency – and increasingly time-domain – systems are widely used in groundwater explorations due to their high-resolving properties and their applicability even in rough terrain. Fixed-wing systems are applicable for reconnaissance surveys in a flat terrain because these systems outrange helicopter-borne systems and they are less expensive but they are less flexible and have less-resolving properties. Frequency-domain systems using natural (e.g., audio-frequency magnetic (AFMAG) systems) sources are not very practicable for detailed groundwater surveys.

On the hardware side most of R&D projects currently focus on HTEM systems. A continuous effort is made to produce HTEM systems having higher moments (larger penetration) while maintaining near-surface resolution using low moments. For the SkyTEM system in particular this is achieved by increasing the transmitter area of the frame, thus approaching a moment of 200 000 Am^2. At the same time a super-low moment has been introduced transmitting current in only one turn achieving the first full off-time gate in 11 μs after begin of turnoff. On-time measurements have been performed for a long time and work is still carried out to improve the data quality but they have yet to prove their usability outside the mineral exploration world. Finally, work is being carried out to improve the noise reduction schemes applied.

On the software side a lot of effort is currently put into more advanced inversion methodologies that match the nature of the subsurface. The spatially constrained inversion is such a new inversion technique. When presenting stitched together 1D soundings the result is often an abrupt variation in neighbouring models because of inherently noisy data and model equivalence. This is a non-optimal result for sedimentary environments where the lateral variations are expected to be smooth. The laterally constrained inversion applies constraints between model parameters along a line to avoid abrupt variations. However, it does not create any connection between neighbouring lines. Features that are perpendicular to flight lines benefit only partially from in-line constraints or smoothing, as no information in the model space is passed between adjacent lines. This means that profile-oriented techniques favour structures following the flight direction. Producing spatial maps based on such methodologies often results in some lineation following the flight paths. The advantage of the spatially constrained inversion approach is that, rather than being filtered or interpolated, information is passed across adjacent flight lines and used to increase model parameter resolution. The approach by Brodie and Sambridge (2006) was somewhat related to the spatially constrained inversion. The utilization of constraints also allows including *a priori* information such as borehole data or data from additional geophysical measurements in the inversion process. This approach not only increases the quality of the inversion results close to the location where sound ground information is available but also spreads this information to distant locations with sparse information density. This integration of diverse sources of data, of both small- and large-scale, into a common interpretation scheme including 1D inversion and 3D forward modelling, seems to be the most promising approach for large-scale groundwater exploration in the near future. And airborne electromagnetic systems will play an increasingly important role, not only for this purpose.

ACKNOWLEDGEMENTS

We would like to thank guest editor Louise Pellerin, the two reviewers and Annika Steuer (LIAG) for reading the manuscript and for their very helpful comments. LIAG is thanked for co-funding the Borkum airborne survey.

REFERENCES

Ahl A. 2003. Automatic 1D inversion of multifrequency airborne electromagnetic data with artificial neural networks: discussion and case study. *Geophysical Prospecting* **51**, 89–97.

Anderson W.L. 1989. A hybrid fast Hankel transform algorithm for electromagnetic modelling. *Geophysics* **54**, 263–266.

Auken E., Christiansen A.V., Jacobsen B.H., Foged N. and Sørensen K.I. 2005. Piecewise 1D laterally constrained inversion of resistivity data. *Geophysical Prospecting* **53**, 497–506.

Auken E., Westergaard J.A., Christiansen A.V. and Sørensen K. I. 2007. Processing and inversion of SkyTEM data for high resolution hydrogeophysical surveys. ASEG 2007, Perth, Western Australia.

Avdeev D.B., Kuvshinov A.V., Pankratov O.V. and Newman G.A. 1998. Three-dimensional frequency-domain modelling of airborne electromagnetic responses. *Exploration Geophysics* **29**, 111–119.

Bakker M., Bosch A. and Gunnik J. 2006. Groningen Valley. In: *Groundwater Resources in Buried Valleys – A Challenge for Geosciences* (eds R. Kirsch, H.-M. Rumpel, W. Scheer and H. Wiederhold), pp. 242–250. Leibniz Institute for Applied Geosciences, Hannover.

Baudouin P., Durozoy G. and Utard M. 1967. Etude par prospection électromagnétic aérienne d'un contact eau douce eau salée dans le delta du Rhône. Mining and Groundwater Geophysics 1967. *Report Geological Survey of Canada* **26**, 626–637.

Beamish D. 2003. Airborne EM footprints. *Geophysical Prospecting* **51**, 49–60.

Beard L.P. 2000. Comparison of methods for estimating earth resistivity from airborne electromagnetic measurements. *Journal of Applied Geophysics* **45**, 239–259.

Beard L.P. and Nyquist J.E. 1998. Simultaneous inversion of airborne electromagnetic data for resistivity and magnetic permeability. *Geophysics* **63**, 1556–1564.

Binley A. and Kemna A. 2005. DC resistivity and induced polarization methods. In: *Hydrogeophysics* (eds Y. Rubin and S.S. Hubbard), pp. 129–156. Springer.

Brodie R. and Sambridge M. 2006. A holistic approach to inversion of frequency-domain airborne EM data. *Geophysics* **71**, G301–G312.

Chen J. and Raiche A. 1998. Inverting AEM data using a damped eigenparameter method. *Exploration Geophysics* **29**, 128–132.

Christensen N.B. 2002. A generic 1-D imaging method for transient electromagnetic data. *Geophysics* **67**, 438–447.

Christiansen A.V., Auken E. and Sørensen K. 2006. The transient electromagnetic method – Airborne TEM. In: *Groundwater Geophysics – A Tool for Hydrogeology* (ed. R. Kirsch), pp. 209–225. Springer.

Christiansen A.V. and Christensen N.B. 2003. A quantitative appraisal of airborne and ground-based transient electromagnetic (TEM) measurements in Denmark. *Geophysics* **68**, 523–534.

Christensen N.B., Halkjær M. and Sørensen K.I. 2008. Mineral and ground water exploration with the SkyTEM system. *Proceedings of the 5th International Conference on Airborne Electromagnetics (AEM2008)*, 28–30 May 2008, Haikko Manor, Finland.

Collett L.S. 1967. Resistivity mapping by electromagnetic methods. Mining and Groundwater Geophysics 1967. *Report Geological Survey of Canada* **26**, 615–624.

Cook P.G. and Kilty S. 1992. A helicopter-borne electromagnetic survey to delineate groundwater recharge rates. *Water Resources Research* **28**, 2953–2961.

Danielsen J.E., Auken E., Jørgensen F., Søndergaard V.H. and Sørensen K.I. 2003. The application of the transient electromagnetic method in hydrogeophysical surveys. *Journal of Applied Geophysics* **53**, 181–198.

Davis A.C., Macnae J. and Robb T. 2006. Pendulum motion in airborne HEM systems. *Exploration Geophysics* **37**, 355–362.

Eberle D.G. and Siemon B. 2006. Identification of buried valleys using the BGR helicopter-borne geophysical system. *Near Surface Geophysics* **4**, 125–133.

Edwards D. and Macaula S. 2008. Airborne electromagnetic surveying for answering environmental/land management questions. A case study from Lower Macquarie catchment, NSW, Australia. *Proceedings of the 5th International Conference on Airborne Electromagnetics (AEM2008)*, 28–30 May 2008, Haikko Manor, Finland.

Effersø F., Auken E. and Sørensen K.I. 1999. Inversion of band-limited TEM responses. *Geophysical Prospecting* **47**, 551–564.

Ellis R.G. 1998. Inversion of airborne electromagnetic data. *Exploration Geophysics* **29**, 121–127.

Ernstson K. and Kirsch R. 2006. Geoelectric methods. In: *Groundwater Geophysics – A Tool for Hydrogeology* (ed. R. Kirsch), pp. 86–108. Springer.

Everett M. and Meju M.A. 2005. Near-surface controlled-source electromagnetic induction: Background and recent advances. In: *Hydrogeophysics* (eds Y. Rubin and S.S. Hubbard), pp. 157–183. Springer.

Farquharson C.G., Oldenburg D.W. and Routh P.S. 2003. Simultaneous 1D inversion of loop-loop electromagnetic data for both magnetic susceptibility and electrical conductivity. *Geophysics* **68**, 1857–1869.

Fitterman D.V. and Deszcz-Pan M. 1998. Helicopter EM mapping of saltwater intrusion in Everglades National Park, Florida. *Exploration Geophysics* **29**, 240–243.

Fitterman D.V. and Yin C. 2004. Effect of bird maneuver on frequency-domain helicopter EM response. *Geophysics* **69**, 1203–1215.

Fluche B. and Sengpiel K.P. 1997. Grundlagen und Anwendungen der Hubschrauber-Geophysik. In: *Umweltgeophysik* (ed. M. Beblo), pp. 363–393. Ernst und Sohn, Berlin.

Fountain D. 1998. Airborne electromagnetic systems 50 years of development. *Exploration Geophysics* **29**, 1–11.

Fountain D. 2008. 60 years of airborne EM – Focus on the last decade. *Proceedings of the 5th International Conference on Airborne Electromagnetics (AEM2008)*, 28–30 May 2008, Haikko Manor, Finland.

Fraser D.C. 1972. A new multicoil aerial electromagnetic prospecting system. *Geophysics* **37**, 518–537.

Fraser D.C. 1978. Resistivity mapping with an airborne multicoil electromagnetic system. *Geophysics* **43**, 144–172.

Gerhardy H. 1975. Probleme der Wasserversorgung auf der Insel Borkum. *Proceedings of the 4th Salt Water Intrusion Meeting (SWIM)*, 31 July 1975, Ghent, Belgium, pp. 30–39.

Haber E., Oldenburg D.W. and Shekhtman R. 2007. Inversion of time domain three-dimensional electromagnetic data. *Geophysical Journal International* **171**, 550–564.

Hodges G. and Siemon B. 2008. Comparative analysis of one-dimensional inversions of Helicopter-borne frequency-domain electromagnetic data. *Proceedings of the 5th International Conference on Airborne Electromagnetics (AEM2008)*, 28–30 May 2008, Haikko Manor, Finland.

Huang H. 2008. Airborne geophysical data levelling based on line-to-line correlations. *Geophysics* **73**, F83–F89.

Huang H. and Fraser D.C. 1999. Airborne resistivity data levelling. *Geophysics* **64**, 378–385.

Huang H. and Fraser D.C. 2003. Inversion of helicopter electromagnetic data to a magnetic conductive layered earth. *Geophysics* **68**, 1211–1223.

Huang H. and Palacky G.J. 1991. Damped least-squares inversion of time-domain airborne EM data based on singular value decomposition. *Geophysical Prospecting* **39**, 827–844.

Huang H. and Rudd J. 2008. Conductivity-depth imaging of helicopter-borne TEM data based on a pseudolayer half-space model. *Geophysics* **73**, F115–F120.

Johansen H.K. and Sørensen K. 1979. The fast Hankel transform. *Geophysical Prospecting* **27**, 876–901.

Jordan H. and Siemon B. 2002. Die Tektonik des nordwestlichen Harzrandes – Ergebnisse der Hubschrauber-Elektromagnetik (The tectonics of the northwestern margin of the Harz Mountains – Results of a helicopter electromagnetic survey). *Zeitschrift der Deutschen Geologischen Gesellschaft* **153**, 31–50.

Jørgensen F., Lykke-Andersen H., Sandersen P., Auken E. and Nørmark E. 2003a. Geophysical investigations of buried Quaternary valleys in Denmark: An integrated application of transient electromagnetic soundings, reflection seismic surveys and exploratory drillings. *Journal of Applied Geophysics* **53**, 215–228.

Jørgensen F., Sandersen P. and Auken E. 2003b. Imaging buried Quaternary valleys using the transient electromagnetic method. *Journal of Applied Geophysics* **53**, 199–213.

Kirsch R. 2006. Hydrogeophysical properties of permeable and low permeable rocks. In: *Groundwater Geophysics – A Tool for Hydrogeology* (ed. R. Kirsch), pp. 1–22. Springer.

Lawry K., Brodie R.C., Clarke J., Tan K.P., Plain C., Wong V., Edwards D., Apps H., Halas L. and Cullen K. 2008. Maximising the value of airborne electromagnetic (AEM) surveys for salinity, land and groundwater management in the River Murray Corridor, South East Australia. *Proceedings of the 5th International Conference on Airborne Electromagnetics (AEM2008)*, 28–30 May 2008, Haikko Manor, Finland.

Macnae J., King A., Stolz N., Osmakoff A. and Blaha A. 1998. Fast AEM data processing and inversion. *Exploration Geophysics* **29**, 163–169.

McNeill J.D. 1980. Electrical conductivity of soils and rocks. Technical Note TN-6, Geonics Ltd, Mississauga, Ontario.

McNeill J.D. 1990. Use of electromagnetic methods for groundwater studies. In: *Geotechnical and Environmental Geophysics, Volume 1* (ed. S.H. Ward), pp. 191–218. SEG.

Munday T. and Fitzpatrick A. 2008. The targeted application of AEM for salinity mapping, interception and disposal: An illustration of the multifarious role of helicopter EM data in environmental management across the Murray Basin of Southeast Australia. *Proceedings of the 5th International Conference on Airborne Electromagnetics (AEM2008)*, 28–30 May 2008, Haikko Manor, Finland.

Newmann G.A. and Alumbaugh D.L. 1995. Frequency-domain modelling of airborne electromagnetic responses using staggered finite differences. *Geophysical Prospecting* **43**, 1021–1041.

Paine J.G., Dutton A.R., Mayorga J.S. and Saunders G.P. 1997. Identifying oil-field salinity sources with airborne and ground-based geophysics: A West Texas example. *The Leading Edge* **16**, 1603–1607.

Paine J.G. and Minty R.S. 2005. Airborne hydrogeophysics. In: *Hydrogeophysics* (eds Y. Rubin and S.S. Hubbard), pp. 333–357. Springer.

Paterson N.R. and Bosschart R.A. 1987. Airborne geophysical exploration for ground water. *Ground Water* **25**, 41–50.

Pignon A. 2008. *3D representations of the freshwater lenses under the island of Borkum – Software comparison for volume estimations*. MsC thesis, Institut EGID Bordeaux 3.

Qian W., Gamey T.J., Holladay J.S., Lewis R. and Abernathy D. 1997. Inversion of airborne electromagnetic data using an Occam technique to resolve a variable number of multiple layers. *Proceedings from the High-resolution Geophysics Workshop, Laboratory of Advanced Subsurface Imaging (LASI)*, University of Arizona, Tucson (CD-Rom).

Röttger B., Kirsch R., Friborg R., Scheer W., Thomsen S. and Voß W. 2005. Multifrequency airborne EM surveys – A tool for aquifer vulnerability mapping. In: *Near-Surface Geophysics* (ed. K.W. Butler), pp. 643–651. SEG.

Rumpel H.-M., Binot F., Gabriel G., Hingsby K., Siemon B., Steuer A. and Wiederhold H. 2006. Cuxhavener Rinne. In: *Groundwater Resources in buried Valleys – A Challenge for Geosciences* (eds R. Kirsch, H.-M. Rumpel, W. Scheer and H. Wiederhold), pp. 227–239. Leibniz Institute for Applied Geosciences, Hannover.

Sasaki Y. 2001. Full 3D inversion of electromagnetic data on PC. *Journal of Applied Geophysics* **46**, 45–54.

Scheer W., Kröger J., Kirsch R. and Zarth M. 2006. Ellerbeker Rinne. In: *Groundwater Resources in Buried Valleys – A Challenge for Geosciences* (eds R. Kirsch, H.-M. Rumpel, W. Scheer and H. Wiederhold), pp. 205–226. Leibniz Institute for Applied Geosciences, Hannover.

Sengpiel K.P. 1983. Resistivity/depth mapping with airborne electromagnetic survey data. *Geophysics* **48**, 181–196.

Sengpiel K.P. 1990. Theoretical and practical aspects of groundwater exploration using airborne electromagnetic techniques. In: *Developments and Application of Modern Electromagnetic Surveys* (ed. D.V. Fitterman), pp. 149–154. US Geological Survey Bulletin 1925.

Sengpiel K.P. and Fluche B. 1992. Application of airborne electromagnetics to groundwater exploration in Pakistan. *Zeitschrift der Deutschen Geologischen Gesellschaft* **143**, 254–261.

Sengpiel K.P. and Meiser P. 1981. Locating the freshwater/salt water interface on the island of Spiekeroog by airborne EM resistivity/depth mapping. *Geologisches Jahrbuch C* **29**, 255–271.

Sengpiel K.P. and Siemon B. 1998. Examples of 1D inversion of multifrequency AEM data from 3D resistivity distributions. *Exploration Geophysics* **29**, 133–141.

Sengpiel K.P. and Siemon B. 2000. Advanced inversion methods for airborne electromagnetics. *Geophysics* **66**, 1983–1992.

Siemon B. 2001. Improved and new resistivity-depth profiles for helicopter electromagnetic data. *Journal of Applied Geophysics* **38**, 65–76.

Siemon B. 2006a. Electromagnetic methods – frequency domain: Airborne techniques. In: *Groundwater Geophysics – A Tool for Hydrogeology* (ed. R. Kirsch), pp. 155–170. Springer.

Siemon B. 2006b. HEM data processing and interpretation at BGR. AEM Workshop on Airborne EM Recent Activities and Future Goals, Hannover, Germany, Expanded Abstracts, 45–49.

Siemon B. 2009. Levelling of frequency-domain helicopter-borne electromagnetic data. *Journal of Applied Geophysics* **67**, 206–218.

Siemon B., Auken E. and Christiansen A.V. 2009. Laterally constrained inversion of frequency-domain helicopter-borne electromagnetic data. *Journal of Applied Geophysics* **67**, 259–268.

Siemon B., Eberle D.G. and Binot F. 2004. Helicopter-borne electromagnetic investigation of coastal aquifers in North-West Germany. *Zeitschrift für Geologische Wissenschaften* **32**, 385–395.

Siemon B. and Greinwald S. 2004. Grundwassererkundung in Namibia mit Hilfe der Hubschrauber geophysik. DVGW energie/wasser-praxis 02/2004, 12-16.

Siemon B., Steuer A., Meyer U. and Rehli H.-J. 2007. HELP ACEH – A post-tsunami helicopter-borne groundwater project along the coasts of Aceh, northern Sumatra. *Near Surface Geophysics* **5**, 231–240.

Siemon B., Stuntebeck C., Sengpiel K.-P., Röttger B., Rehli H.-J. and Eberle D.G. 2002. Investigation of hazardous waste sites and their environment using the BGR helicopter-borne geophysical system. *Journal of Environmental & Engineering Geophysics* **7**, 169–181.

Smith R.S., O'Connell M.D. and Poulsen L.H. 2004. Using airborne surveys to investigate the hydro-geology of an area near Nyborg, Denmark. 74th SEG meeting, Denver, Colorado, USA, Expanded Abstracts.

Smith B.D., Sengpiel K.P., Plesha J. and Horton R.J. 1992. Airborne electromagnetic mapping of sub-surface brine, Brookhaven Oil Field, Mississippi. 62nd SEG meeting, New Orleans, Louisiana, USA, Expanded Abstracts, 340–343.

Sørensen K.I. and Auken E. 2004. SkyTEM - A new high-resolution helicopter transient electromagnetic system. *Exploration Geophysics* **35**, 191–199.

Steuer A., Siemon B. and Eberle D. 2008a. Airborne and ground-based electromagnetic investigations of the fresh-water potential in the tsunami-hit area Sigli, northern Sumatra. *Journal of Environmental & Engineering Geophysics* **13**, 39–48.

Steuer A., Siemon B. and Viezzoli A. 2008b. Application of spatially constraint inversion on HEM and SkyTEM data. *Proceedings of the 5th International Conference on Airborne Electromagnetics (AEM2008)*, 28–30 May 2008, Haikko Manor, Finland.

Valleau N. 2000. HEM data processing – A practical overview. *Exploration Geophysics* **31**, 584–594.

Viezzoli A., Christiansen A.V., Auken E. and Sørensen K.I. 2008a. Quasi-3D modeling of airborne TEM data by spatially constrained inversion. *Geophysics* **73**, F105–F113.

Viezzoli A., Siemon B., Christiansen A.V. and Auken E. 2008b. Spatially constrained inversion of HEM data: The Banda Aceh case study. *Proceedings of the 5th International Conference on Airborne Electromagnetics (AEM2008)*, 28–30 May 2008, Haikko Manor, Finland.

Wait J.R. 1982. *Geo-electromagnetism*. Academic Press.

Ward S.H. and Hohmann G.W. 1988. Electromagnetic theory for geophysical applications. In: *Electromagnetic Methods in Applied Geophysics. Volume 1: Theory* (ed. M.N. Nabighian), pp. 130–310. SEG.

Weidelt P. 1991. *Introduction into electromagnetic sounding*. Lecture manuscript, Technical University of Braunschweig.

Worzyk P. 1995a. Geoelektrische Tiefensondierungen auf der Insel Borkum – Untersuchungen zur Veränderung der Süßwasserlinse im Ostland. NLfB Archives No. 111751, Hannover.

Worzyk P. 1995b. Geoelektrische Tiefensondierungen auf der Insel Borkum – Untersuchungen zur Struktur der Süßwasserlinse im Einzugsbereich des Gewinnungsgebietes Waterdelle. NLfB Archives No. 114088, Hannover.

Wynn J., Bultman M. and Lemieux J. 2005. Airborne geophysics versus groundwater – An example. In: *Near-Surface Geophysics* (ed. K.W. Butler), pp. 635–641. SEG.

Xiong Z. and Tripp A.C. 1995. Electromagnetic scattering of large structures in layered earth using integral equations. *Radio Science* **30**, 921–929.

Yin C. and Fraser D.C. 2004. Attitude corrections of helicopter EM data using a superposed dipole model. *Geophysics* **69**, 431–439.

Yin C. and Hodges G. 2005. Influence of displacement currents on the response of helicopter electromagnetic systems. *Geophysics* **70**, G95–G100.

Yin C. and Hodges G. 2007. Simulated annealing for airborne EM inversion. *Geophysics* **72**, F189–F195.